ADVANCED COURSE ON STRUCTURAL CONTROL AND HEALTH MONITORING
SMART'01 – (PP.425–447) – WARSAW, MAY 22-25, 2001.

Monitoring of stress changes with ultrasound

J. SZELĄŻEK and J. DEPUTAT

Ultrasonic Testing Laboratory,
Institute of Fundamental Technological Research
Świętokrzyska 21, 00-049 Warszawa, Poland

The paper describes applications of ultrasonic technique for stress monitoring in various construction elements. In the introduction other nondestructive stress measurement methods are presented and compared to ultrasonic technique. Elastoacoustic effect (dependence of ultrasonic wave velocity on stress) is described for various ultrasonic waves propagated in steel. Presented are two techniques of ultrasonic pulse time of flight measurement, used for ultrasonic stress monitoring. The first one, based on acoustic birefringence evaluation, is used for monitoring of thickness averaged stress. The second one, based on the measurement of time of flight of longitudinal subsurface wave, is used for stress evaluation in the surface layer of the material. Results of tests performed with this technique can be compared to results obtained with well known resistance strain gauges. Paper describes examples of industrial application of ultrasonic stress evaluation. Described are results of measurements performed on monoblock railroad wheels, where ultrasonic technique was used for monitoring of hoop residual stress development due to braking applications. These results were compared with results obtained using X-ray diffraction technique and destructive tests (radial saw cut technique). Wheels under test were subjected to braking applications both on the stand and in the track. The second example describes measurements of longitudinal component of residual stress in railroad rails after straightening. In this case ultrasonic test data were compared with destructive stress measurements and strain gauges. The last example describes results of longitudinal force monitoring in the continuously welded rails, in the track. Stresses monitored were due to thermal expansion of the rail material (thermal stress) and due to longitudinal displacement of the rail due to service loads. All presented in the applications measurements were performed with portable devices developed for precise measurement of ultrasonic pulse time of flight.

1. Introduction

There are many branches of technology which need fast and nondestructive evaluation of both applied and residual stresses. The sum of these stresses can decisively influence the state of the element of the machine or a structure. A well known example of such dangerous stresses are welding stresses created during assembling of rigid structures like tanks. High residual stresses in such structures can lead to cracking or construction deformation. Another example are residual stresses in the massive, revolving shafts. During service, the inhomogeneous residual stress, introduced into the shaft material during manufacturing or repair, can result in shaft deformation. In case of main propeller shaft in the ship such deformation means very expensive repair. High tensile residual hoop stress in the rim of monoblock railroad wheel can lead to wheel failure and in railroad community wheels with very high hoop residual stresses are called "explosive".

To monitor or evaluate stresses numerous nondestructive or quasi nondestructive methods were developed. Destructive techniques, based on the displacement due to stress relieving measured in course of element cutting or sectioning, are used for residual stress evaluation. They are usually very laborious and expensive (also the element under test is destroyed).

Some of nondestructive techniques, like Barkhausen noise technique or X-ray diffraction, have a long history and found numerous industrial applications. But these methods are able to evaluate surface stress only. They also need very careful surface preparation or results are influenced by plastic deformation of material surface what can be often observed during service. This was the reason why Barkhausen noise technique failed when applied to the stress measurements in monoblock wheels which surfaces during service are subjected to local mechanical deformations.

The most popular technique of stress monitoring is based on resistance strain gauges. They are used for measurement of deformation on the material surface what allows to calculate surface stress. Their disadvantage, in some application, is that delicate gauges glued to the material surface must stay on it all the time. If the object under test is subjected to heating for example, gauges usually are destroyed.

Paper describes theoretical background and applications of a nondestructive, ultrasonic technique of stress monitoring. This technique, not so accurate however like resistance strain gauges method, can replace them in several situations. Examples of applications present such cases where industrial experiences showed that ultrasonic technique provides with valid results.

2. Ultrasonic stress evaluation

The dependence of ultrasonic waves velocity on stress yielded on the material is called the elastoacoustic effect. Ultrasonic stress measurements are based on this effect. The theoretical description of stress-velocity dependence is given by the nonlinear theory of elasticity [1].

The wave velocity depends on the material elastic constants. In the linear theory of elasticity the elastic constants and the wave velocity do not depend on elastic strain. The second and higher order elastic constants however depend on strain and they connect small amplitude elastic wave velocity with stress [2].

Figure 1 presents results of measurements performed on the steel sample during tensile test. Measured were time of flight (TOF) of ultrasonic pulses in the sample material over the determined distance. The aim of measurement was to determine the dependence TOF – stress. The diagram shows the comparative changes of TOF for various ultrasonic waves propagated in various directions in respect to stress.

The stress-velocity dependence in compression is simply the extrapolation of lines describing the dependence in tension.

The "sensitivity" of the ultrasonic wave to stress is described by elastoacoustic constant. The value of this constant is calculated as:

$$\beta_{ijk} = \frac{V - V_o}{V\sigma} = \frac{t_o - t}{t\sigma},$$

where:

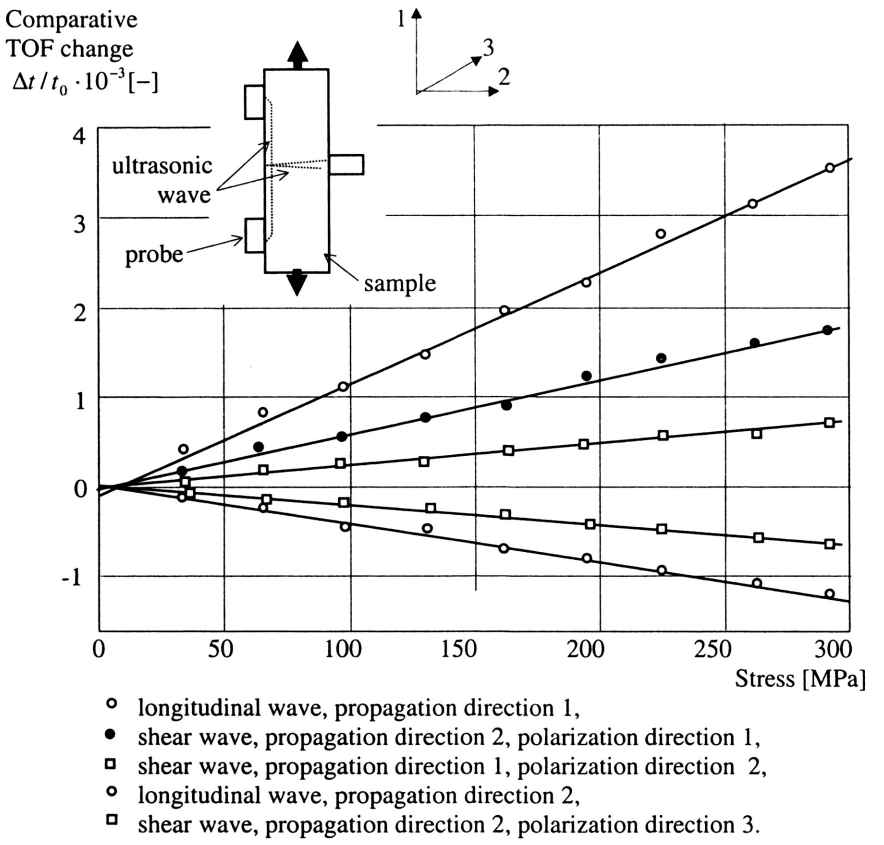

FIGURE 1. Results of measurements of ultrasonic pulses time of flight (TOFs), for various wave types and directions of propagation on the steel sample subjected to tension.

V and V_o – phase velocities in stress free and stressed medium respectively,
t and t_o – times of flight in stress free and stressed medium respectively,
β_{ijk} – elastoacoustic constant, indices i, j, and k denote direction of wave propagation, wave polarization and stress,
σ – stress.

It can be seen that the most "sensitive" to stress is longitudinal wave propagated along the stress. The second high elastoacoustic constant wave is shear wave propagated perpendicular and polarized parallel to stress. These two waves are most often used in ultrasonic tensometry.

Values of elastoacoustic constants for various ultrasonic waves propagated in steel are presented, as an example, in the Table 1 [3].

TOF changes due to stress are, unfortunately, small. In the most expedient case of longitudinal wave propagated parallel to stress in steel, the increment of tensile stress by 10 MPa causes the increase of TOF by 0.0125% only. This TOF change is equivalent to velocity decrease by 0.74 m/s. Assuming the possible maximum change of stress in steel

TABLE 1. Elastoacoustic constants for steel.

Wave type	Direction of wave propagation	Direction of wave polarization	Elastoacoustic constant [MPa^{-1}]
longitudinal	parallel to stress	—	$-1.25 \cdot 10^{-5}$
shear	perpendicular to stress	parallel to stress	$-0.79 \cdot 10^{-5}$
shear	parallel to stress	perpendicular to stress	$0.14 \cdot 10^{-5}$
longitudinal	perpendicular to stress	—	$+0.13 \cdot 10^{-5}$
shear	perpendicular to stress	perpendicular to stress	$+0.02 \cdot 10^{-5}$

construction member from -500 MPa to $+500$ MPa one can extract the corresponding velocity change of longitudinal wave propagating in the direction of stress of the range of 74 m/s. Such change of velocity, when measured over the distance 200 mm in steel, causes the change of TOF of the order of 400 ns. Therefore in ultrasonic stress measurements TOFs has to be measured with a very high, 10^{-9} (nanosecond) accuracy. It means that in ultrasonic tensometry special equipment and special sets of ultrasonic probes have to be used.

Most of technical materials are anisotropic. It is result of manufacturing processes like rolling, casting or forging. During these operations grains of metal become preferred oriented creating texture. In anisotropic materials velocity of waves propagation depend on direction of propagation versus acoustic axes determined by texture directions. Velocity changes due to texture can be even higher than those due to stresses and elimination of texture influence on results of ultrasonic tensometry is a great challenge.

A linear velocity-stress dependencies in anisotropic media are observed only for waves propagated along the acoustic axis of a medium. In practice this fact limits the applications of ultrasonic tensometry for elements in which directions of texture and main stresses coincide. In practice such coincidence is observed in numerous construction members like steel beams subjected for tension, compression or bending and pipes subjected to bending or internal pressure. In these elements the direction of texture due to rolling and direction of main stresses are parallel or perpendicular to element beam or pipe axis.

If the absolute value of stress is to be evaluated the only practical way to eliminate the influence of texture on readings is calibration of the measuring device on stress free sample. Calibration sample has to be made of the material exhibiting the same chemical composition and texture as the object to be tested. Such approach can be used for test on objects manufactured in series, in a repetitive way like railroad rails or wheels. In such cases the calibration sample can be made of a piece of the rail or wheel subjected to stress relieving annealing. During calibration TOFs in zero stress state are measured. The difference between calibration sample TOF and element under test TOF is proportional to stress value.

If the stress changes are to be evaluated the texture of the material does not influence ultrasonic readings. Measurements in such a case are repeated at the same location and one can assume that the texture of material is constant and the only factors influencing velocities of ultrasonic waves are stress and temperature changes. Temperature dependence of ultrasonic wave velocity can be easily measured and temperature independent TOFs can be calculated.

3. Techniques of ultrasonic measurements

There are two techniques of stress measurement which found today practical applications. The first one, and the oldest, uses shear waves propagating in the thickness direction and can be used on plane-parallel objects like plates, pipe walls etc. With this technique acoustic birefringence can be measured. The advantage of this technique is no need to know exact thickness of the tested element and possibility to evaluate stress value averaged over the element thickness.

The second technique uses subsurface waves and can be used on objects with flat surfaces and on cylinders like shafts or pipes when the wave propagate along the cylinder axis. Longitudinal subsurface wave is sensitive to stress component parallel to its propagation direction and is used to determine the value of stress in the thin, surface layer of the material. Results of measurements can be compared to resistance strain gauges readings. Subsurface shear SH wave (polarization direction parallel to the element surface) is sensitive to stress component perpendicular to the wave propagation direction. When propagated together with longitudinal wave along the cylinder axis these two waves allow to determine both longitudinal and circumferential stress components in the cylinder wall.

With these two techniques stress averaged over the element thickness and stresses on both element surfaces can be evaluated. In elements subjected to bending or tension and bending, one can determine approximate stress distribution in the object cross section. Such an example is presented in section 4.1 describing hoop stress distribution in the rim of monoblock, cast wheel.

3.1. Acoustic birefringence measurement

The principle of measurement with shear waves propagating in the thickness direction is shown in Fig. 2. Ultrasonic probehead, positioned on one of the surfaces, generates shear wave in the direction perpendicular to the surface. The wave reflects on the opposite surface and is detected by the probehead working in the echo mode. For low attenuating materials, like steel, several "echoes" (reflections of the pulse between top and bottom surfaces) can be observed and used for TOF measurement.

The polarization direction of the wave can be changed (by rotating the probe or using multitransducer probes) and TOFs for two perpendicular polarizations can be measured. One polarization has to be parallel to stress direction, the second one – perpendicular to stress. Acoustic birefringence is proportional to the difference between velocities of waves polarized in these two directions and is calculated as:

$$B = B_A + B_\sigma = \frac{2(V_1 - V_2)}{V_1 + V_2} = \frac{2(t_2 - t_1)}{t_1 + t_2},$$

where:
B_A – birefringence due to texture (initial anisotropy or zero stress anisotropy),
B_σ – birefringence due to stress,
V_1 and V_2 – velocities of shear waves polarized in two perpendicular directions 1 and 2,
t_1 and t_2 – times of flight of waves polarized in directions 1 and 2.

If the absolute stress value is to be evaluated, the value of B_A has to be determined experimentally on stress relieving annealed sample exhibiting the same texture induced anisotropy as the element under test.

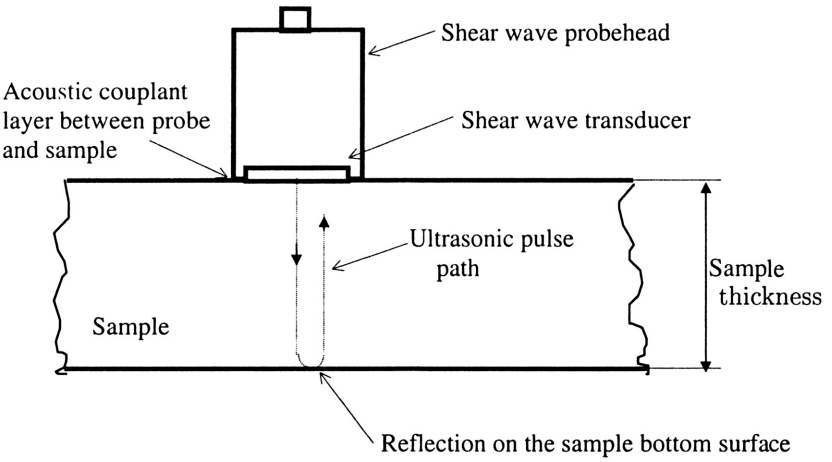

FIGURE 2. Measurement of acoustic birefringence in plate like object. Ultrasonic shear waves propagate in the thickness direction.

The advantage of this technique of stress evaluation is that the thickness of the object has not to be precisely known. The second important feature of birefringence technique is that the result is in practice temperature independent. TOFs measured as shown in Fig. 5 are temperature influenced due to thermal expansion of the material thickness increase) and temperature induces pulse velocity changes. Since both waves are shear waves and they propagate in the same material volume, temperature induced thickness changes and wave velocity changes are in practice the same for both of them.

3.2. Measurement of time of flight for subsurface waves

The second technique of TOF measurement is the use of subsurface waves. These waves propagate along the flat material surface and can be generated and detected from the same surface. The schema of subsurface pulses TOF measurement is shown in Fig 3. For generation and detection of subsurface waves probes equipped with plastic wedges are used. For longitudinal subsurface wave the wedge angle is equal to the first critical angle.

Probe wedges are acoustically coupled to the element surface with a liquid. The thickens of couplant layer depends on local surface roughness. To eliminate unwanted influence of coupling variations on measured TOFs multitransducer set of probes are used. The elementary set consists of one transmitting probe and two receiving probes arranged in one line. Measured are two TOFs: between Transmitter and Receiver 1 and between Transmitter and Receiver 2. The difference between these two measured TOFs gives time of flight of the pulse in the sample material, over the distance L, eliminating times of flight in plastic consists of several elementary sets. With such sets precise TOFs measurements can be performed on flat or cylindrical rough surfaces without any time consuming surface preparation [4].

TOFs of subsurface waves are significantly influenced by temperature changes due to high temperature dependence of ultrasonic wave velocity in the plastic wedges. Also

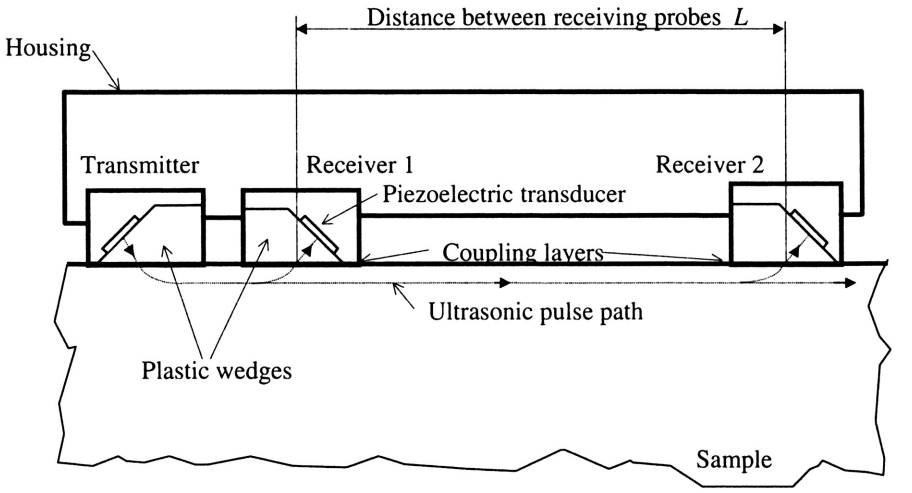

FIGURE 3. Elementary set of probes for TOF measurement of subsurface waves.

the distance between receiving probes (L on the Fig. 3), due to thermal elongation of the probe housing, is temperature dependent. To eliminate the unwanted temperature influence on readings, temperature TOF dependence has to be measured experimentally for each set. During stress evaluation thermal correction has to be taken into account. This correction is the sum of the TOF changes due to temperature velocity change in the material under test and all temperature phenomena observed in the set of probes. Its value vary depending on the material under test (carbon steel, alloy steel, light alloys). It is worth mentioning that in some cases, when the measurements has to be carried in a wide range of temperatures, the temperature effects can be several times higher than TOF changes caused by stress.

4. Practical applications of ultrasonic stress evaluation

Chapter describes examples of practical application of ultrasonic stress measurements. All objects tested are heavy steel elements with partly flat surfaces enabling generation and detection of ultrasonic waves. In all of them one component of stress was dominant and it was assumed that they are subjected to tension or compression only.

4.1. Monitoring of hoop residual stress development in the monoblock railroad wheels

The majority of railroad wheels in service today are monoblock wheels (made of one piece of steel). During service the rim of the railroad wheel is subjected to heating resulting from the friction between braking block and the rim thread. Nonuniform heat impacts in the wheel lead to the development of tensile hoop stress in the wheel rim. If the crack in the rim is present tensile hoop stress acts as a crack driving force and can

result in the rim fracture. Therefore stress state in the rim should be monitored and wheels exhibiting high tensile stress has to be removed from service.

For stress evaluation in the wheel rim two ultrasonic techniques can be applied. Figure 4 shows position of the shear wave probe on the wheel rim, used for the measurement of acoustic birefringence. Value of the birefringence, assuming the rim texture is known and the rim is subjected to hoop stress only, allows to evaluate hoop stress value averaged over the rim thickness. Figure 5 presents the set of probes used for generation of subsurface waves along the rim faces, in the hoop direction. Results obtained with this technique, on both rim faces, provide information about hoop stresses in the surface layer on both faces.

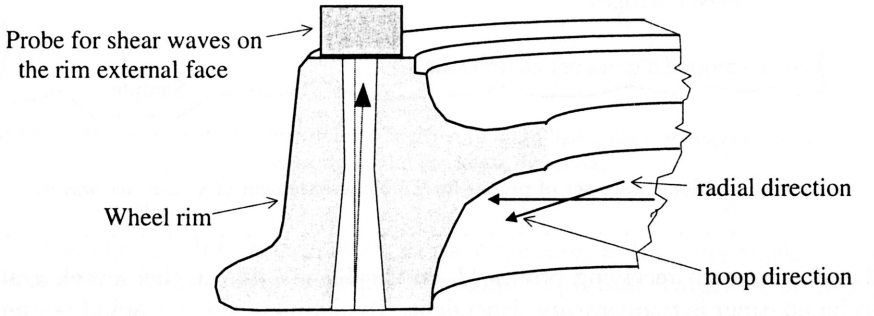

FIGURE 4. Measurement of acoustic birefringence in the rim of monoblock railroad wheel. Position of the ultrasonic probe on the rim external face.

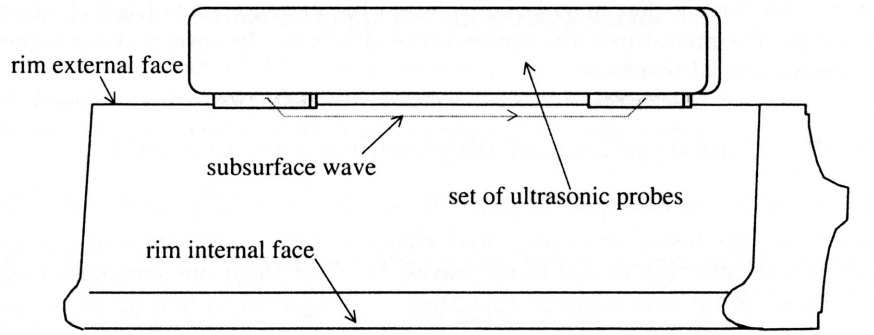

FIGURE 5. Measurement of subsurface waves TOF. Set of probes on the rim external face.

The use of both measuring techniques, described earlier, allows to predict not only net rim force proportional to the hoop stress averaged over the rim cross section, but also the distribution of hoop stress over the rim thickness.

Figure 6 shows results of hoop stress monitoring performed with ultrasonic and X-ray diffraction technique on one wheel during braking in the stand. The wheel was subjected

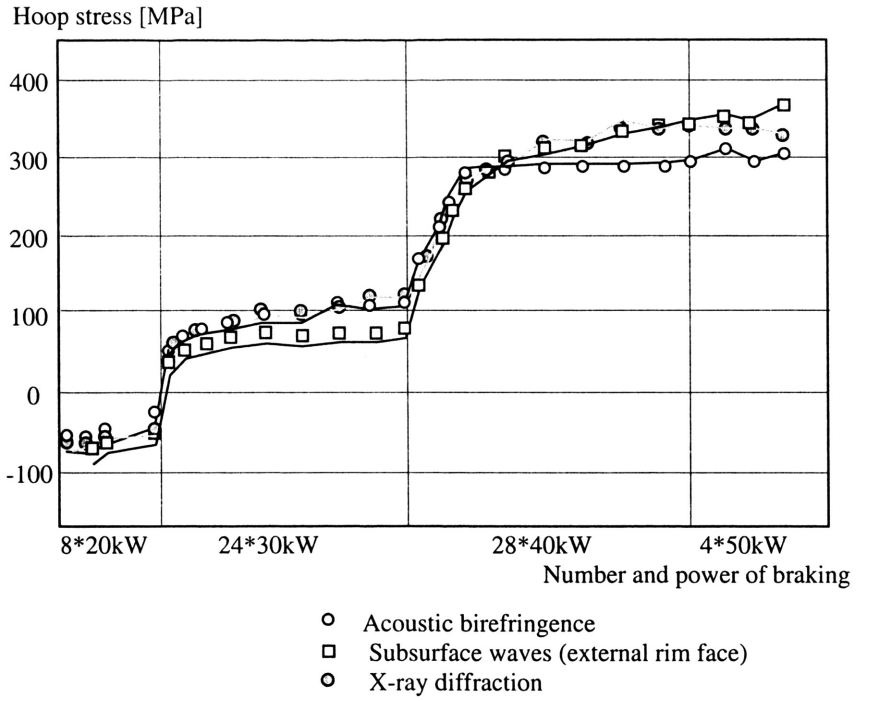

FIGURE 6. Results of measurements performed on monoblock wheel subjected to numerous braking applications in the stand. Comparison of ultrasonic and X-ray diffraction results. (Measured in Vitry, France [6]).

to 64 braking cycles and the duration of each cycle was 1 hour. The braking shoe was in a central position. Ultrasonic readings were taken after each braking application, after cooling the wheel to the room temperature. Before the measurement the device was calibrated on stress relieving annealed rim block what allowed to measure not only stress changes but also its absolute value.

It can be seen that in the as manufactured wheel hoop residual stress is compression and equal to about −50 MPa. Starting power of braking was 20 kW and the maximum power was 50 kW. Brakings with 20 kW power do not change the stress state. Significant stress increments are observed after first 30 and 50 kW brakings. The maximum tensile stress measured after last braking application was about 480 MPa.

It can be also seen that stress values on the external rim face and averaged over the rim thickness are similar. Measurements performed with X-ray diffraction on the rim external face confirmed data obtained with ultrasonic technique.

Next drawing, Fig. 7, presents result of ultrasonic measurements performed on the second wheel subjected to braking in the stand. Ultrasonic readings were taken in three points spaced 120° to check stress distribution one the wheel circumference. The braking started with the maximum power and a significant hoop stress increment can be seen after the first braking cycle. The same stress values in all measuring points proved that hoop stress is distributed evenly on the rim circumference.

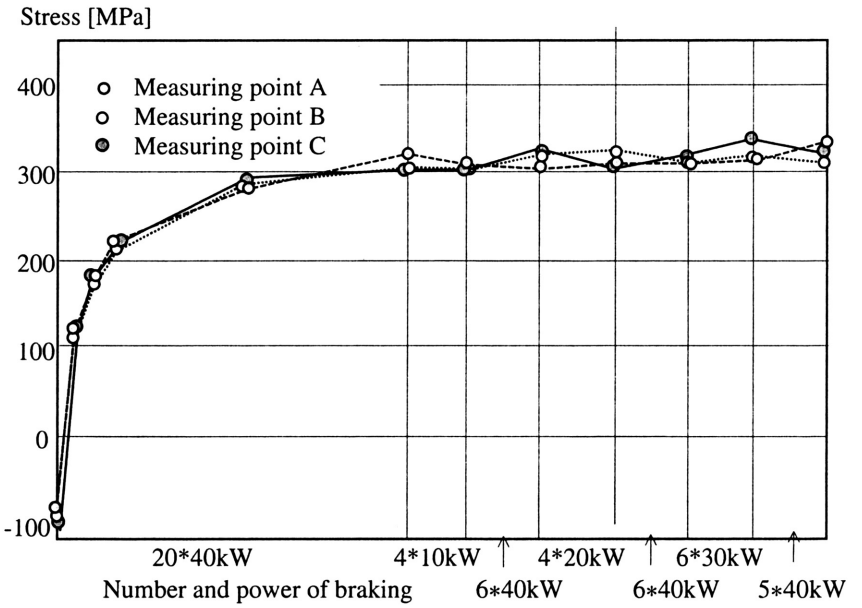

FIGURE 7. Results of measurements performed on monoblock wheel subjected to numerous braking applications in the stand. Measurements in three positions on the rim circumference. (Measured in Vitry, France [6]).

During braking in the stand the wheel is cooled only by the air in the braking chamber and its temperature can reach more than 500°C. Wheels on the track are in constant contact with the relatively cool rail. In result wheel temperature during braking on track is lower and hoop stress development is slower than in the stand. Figure 8 presents result of the first field measurements of hoop stress development in the wheel during braking on track. Wheels under test were installed in the standard wagon, power of braking and wheel temperature were controlled in the test car. Braking duration was about 1 hour, wagon speed – about 100 km/hour. Ultrasonic tests were performed during stops after each braking cycle. Readings were taken on two points on the rim circumference. Measured were both acoustic birefringence and subsurface waves TOFs on the rim front face.

In contrast to results showed in Figs. 6 and 7 significant differences between thickness averaged and surface stresses can be seen. These differences were caused by changing of braking shoe position on the wheel rim during braking. During first runs breaking shoe was overhanging (close to the front rim face), than it was overriding (close to the wheel flange). Depending on the shoe position, the temperature in the various regions of the rim were different what resulted in differences between averaged and surface stresses.

The rim temperature was monitored during brakings. The maximum temperature for each braking cycle is presented also in Fig. 8. Correlation between hoop stress increment and the maximum rim temperature can be noticed.

Data presented in Figs. 6-8 are result of a research program organized by International Railway Union in 1987. Measurements with X-ray diffraction and brakings in the

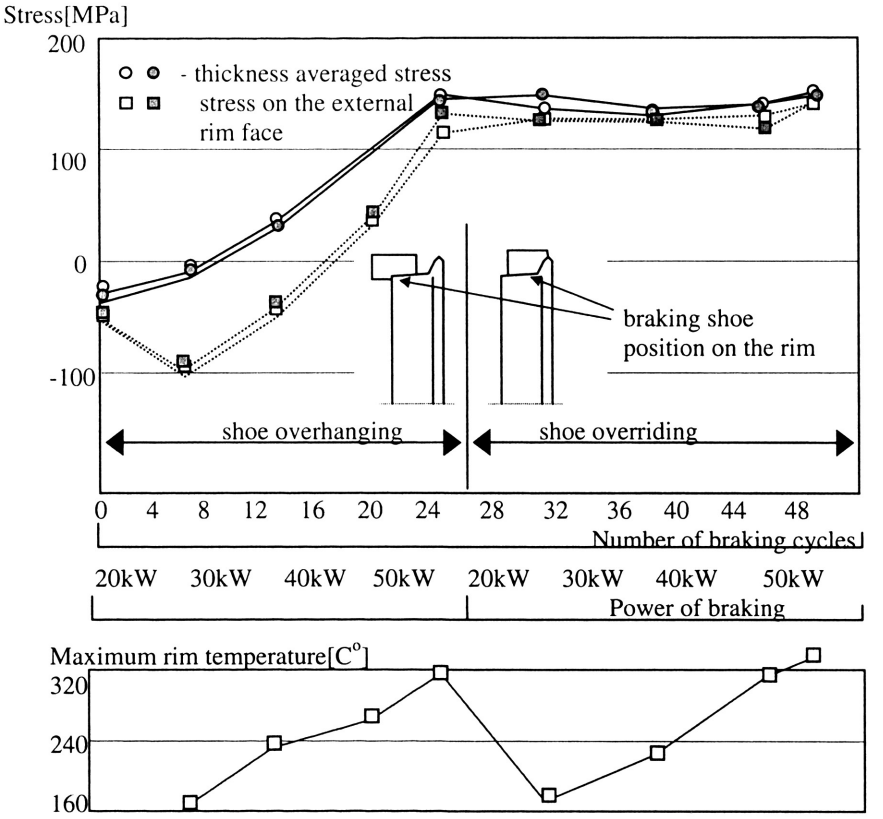

FIGURE 8. Results of measurements performed during braking on track. (Measured in Velim, Czech Republic [6]).

stand were performed by French team, brakings on the track by Czech and German teams. Ultrasonic measurements were taken by Ultrasonic Testing Laboratory, IFTR, Warsaw.

When hoop stress values on both rim faces and stress averaged over the rim thickness are known one can predict hoop stress distribution in the rim cross section. Such measurements were performed on American cast wheels. Figure 9 shows possible stress distributions in 4 wheels subjected to heating with various power. In as manufactured wheels stress is compressive. After heating surface stress on the rim external face becomes more compressive, the same time surface stress on the external value becomes tensile. Changes of stress averaged over the rim thickness are small. It means that after heating the rim of the wheel is subjected not only to tension but also to bending. This different, as compare to European wheels, stress development is due to conical shape of the standard cast wheel plate. Tensile stress in the rim leads to plate deformation creating bending momentum in the rim. Bending results in the development of compressive stress on the external face and tensile stress on the external face as shown on Fig. 9.

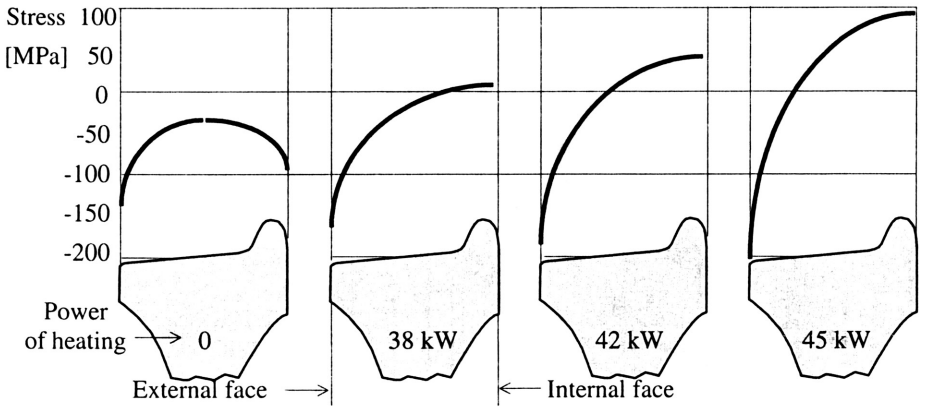

FIGURE 9. Probable hoop stress distributions in the rim of standard cast wheel subjected to heating in the coil. (Based on results of measurements in Boulder, Colorado [7]).

Hoop stress distribution as presented in Fig. 9 was confirmed during destructive tests performed on some wheels. Stressed wheels were cut in radial direction and during cutting the cut opening displacement was measured on both rim faces. Cut closing displacement was observed on the external face and opening of the cut on internal face.

Such stress distribution and plate deformation was also predicted by theoretical analysis of the wheel thermal loads [8].

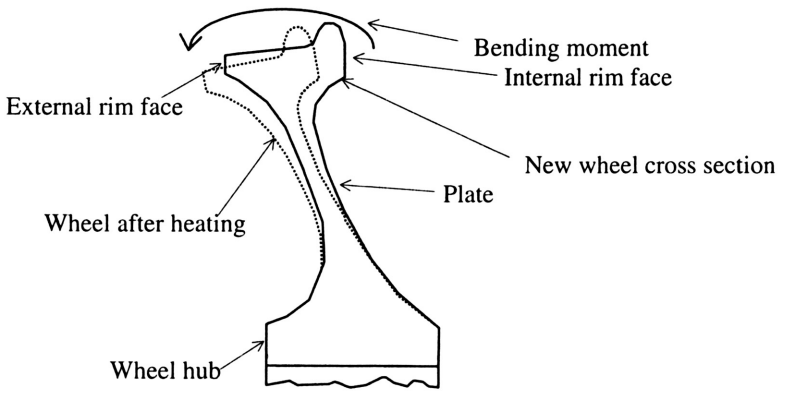

FIGURE 10. Deformation of the standard cast wheel due to thermal loads.

4.2. Monitoring of longitudinal forces in the continuously welded rail (CWR)

Longitudinal forces in the CWR are mostly the result of thermal stress and stress due to longitudinal rail displacement. The rail displacement is result of longitudinal loads

applied to the CWR by braking or accelerating trains. Longitudinal CWR displacements can be also observed when the temperature along the CWR significantly differs due to uneven sun operations. As a result of all three mentioned stress sources in the CWR, the rails are subjected to longitudinal forces which values change in the time, in day-night cycle, depend on the weather, track design and on the track bed stiffness. In some places on the track, before stop signs for example, continuous rise of compressive force can be expected. Forces in each rail can be different what can lead to track buckling in lower temperature than expected.

For longitudinal force monitoring subsurface longitudinal wave propagated along the rail was used. It can be assumed that during the service of the rail in CWR material texture, chemical composition and residual stresses on the rail head external side or in the rail foot are constant. The only factors influencing the velocity of longitudinal wave in the given location on the rail are rail temperature, thermal stress and longitudinal stress due to rail displacement. Probehead for longitudinal subsurface wave can be used as a "ultrasonic stress gauges" for periodic measurement of force changes in a selected positions along the CWR.

The absolute force value can be measured assuming that the first measurement, called calibration, is performed on longitudinal force free rail.

Figure 11 presents results of measurement performed with longitudinal, subsurface wave propagated along the rail. Multitransducer probe, 2 MHz frequency were used to measure time of flight of ultrasonic pulses over the distance of about 300 mm. Measurement were performed every 10 ton force increment corresponding to stress increment

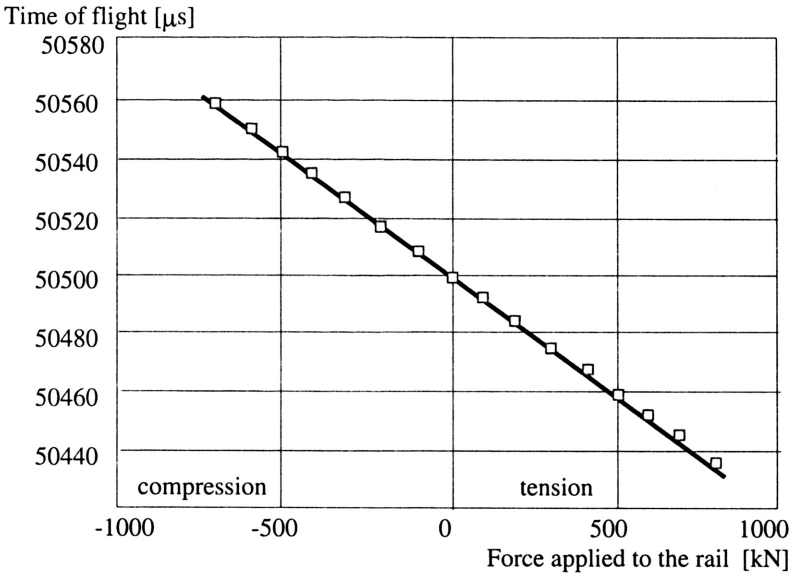

FIGURE 11. The dependencies between time of flight of longitudinal subsurface wave propagated along the rail and longitudinal force applied to the rail.

equal to about 13.5 MPa. It can be seen that for this measuring distance, stress change equal to 1 MPa results in the time of flight increment equal to about 1.5 ns.

Measurements of the dependence thermal stress – temperature

It can be calculated that, assuming the absence of longitudinal rail displacement, the CWR temperature change equal to 1°C results in thermal stress increment equal to 2.5 MPa. For UIC-60 rail, with cross section equal to 7686 mm^2, it correspond to thermal force equal to 18.6 kN. In Central Europe rail temperature changes from −30°C to +60°C. In extreme climate condition rail temperature can change in range of 120°C. It means that thermal force in the rail can reach up to 300 tons!

If the rail can move in the longitudinal direction during thermal stress build-up, stress increments will be lower. The aim of the tests was to measure what are the stress changes resulting from 1°C rail temperature increment and how they depend on the track state and location.

Figure 12 shows thermal stress changes measured during one day on a straight, subjected to sun operation and well maintained UIC-60 CWR. It can be seen that measured stress changes are linear and very close to theoretical predictions. It means that there was no longitudinal displacement of the rail during the day temperature changes.

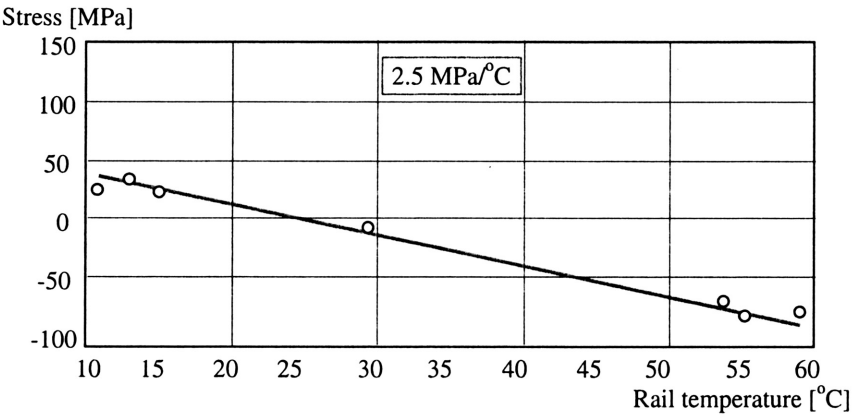

FIGURE 12. Thermal stress – rail temperature relation measured on the straight CWR.

Figure 13 presents results of measurements performed on the CWR close to the bolted joint. The rail surfaces in the joint exhibited marks of rail ends displacement. During the measurement the displacement of few millimeters in the joint was noticed. Thermal stress change, for 1°C rail temperature increment, measured in this rail was equal to 1.75 MPa. Lower MPa/°C ratio is a result of partial release of thermal stress. Displacements were taking place in numerous small steps when the thermal stress reached higher value than the friction force in the joint.

Similar measurements were performed for a longer time period in the USA [9]. Results showed also that the thermal stress-temperature relation depends on the location

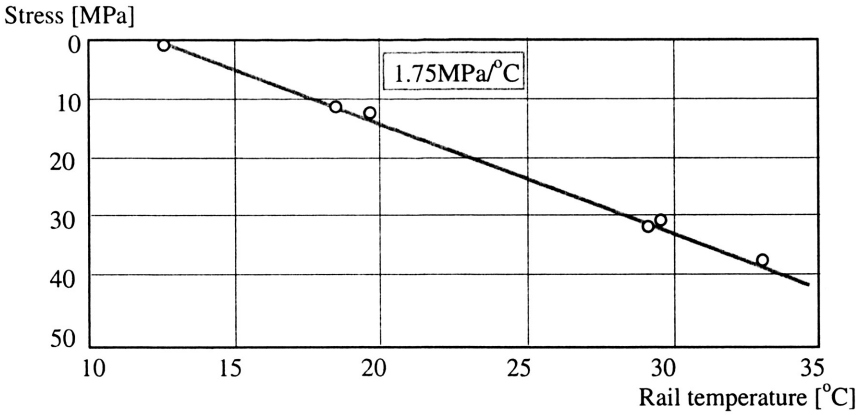

FIGURE 13. Thermal stress - rail temperature relation measured close to the bolted joint.

and seems to be a characteristic feature of the given CWR section. Stress-temperature factor equal to 2.6 MPa/°C was measured close to the road crossing. In the distance from the road crossing 1.9 MPa/°C thermal stress changes were observed. Figure 14 shows data collected during similar measurements but performed in numerous locations along the CWR partially and temporarily shadowed by trees, in the distance 200 m from the switch [10]. Diagram presents the distribution of thermal stress changes caused by 1°C rail temperature increment (vertical axis) along the rail (horizontal axis). In general stress-temperature ratio for this track section is higher than theoretically predicted

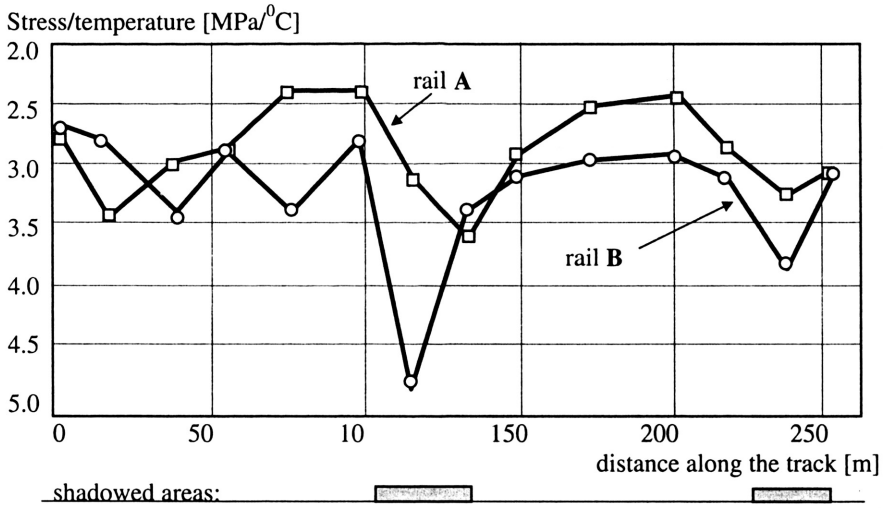

FIGURE 14. Thermal stress changes along both rails of the track partly in the shadow.

and the mean value of this ratio is equal to about 3.7 MPa/°C. The reason of such a high thermal stress increment is not explained. However it can be noticed that minima of stress-temperature ratio are located in the same regions in both rails corresponding with shadowed regions. High stress increments in these parts of the track can be explained by small, measured in millimeters, longitudinal rails displacements. In the morning, when parts of the track were in shadow, thermal stress builds-up in the rail regions subjected to sun operation. Thermal stress caused longitudinal rail displacement towards shadowed parts, where thermal stresses were lower. In the midday, when all length of the track was in the sun, thermal stresses started to build-up also in the regions previously in the shadow. In these regions thermal stress and stress from rail displacement summed up. It resulted in the highest stress-temperature factors for these track regions. Numerous passing trains, vibrating rails, helped the rails to move in the longitudinal direction.

Rail neutral temperature

It is assumed that at the so called neutral (or zero force) temperature, longitudinal force in the CWR is equal to zero. The neutral temperature of the rail is the one measured during the closure welding. One such weld can close a rail sector up to 400 m long. It was observed that the rail temperature changes during construction works, depending on the weather and sun operation. If some parts of the rail section are in the shadow, their neutral temperature can be higher than those of the rail in the sun. During construction of a new track, after the last closure welding, the geometry of the track is adjusted. It means that the track is displaced both in vertical and horizontal directions. All mentioned factors result in variations of the neutral temperature (or longitudinal force) along the CWR. The aim of presented measurements was to check what are the longitudinal forces in the CWR at neutral temperature and what is their distribution along the CWR.

The measurements were performed in thirteen locations on each rail, on 400 m long track section [11]. The first series of measurements were performed on the external force free rail, laying on the ties. It was assumed that during the first measurements the longitudinal force in the rail was equal to zero. The measurements of the second series were taken in the same locations but after fixing of the rails to the ties, welding into the CWR and track geometry regulation. Intentionally all measurements were performed for almost the same rails temperature, equal to neutral temperature. It means that the difference between first and second readings is not due to thermal stress but due to forces introduced into the rails during fixing them to the ties and track geometry regulation. Thermal stress which could occur in the rails was evaluated as lower than ±5 MPa.

Results of the measurements are presented in Fig. 15. Vertical axis of the diagram presents longitudinal stress in the rail, horizontal – position of the measuring location along the rail.

It can be seen that mean value of stresses measured in both rails are close to zero. They are distributed in similar way along the track in both rails and vary from −25 up to +30 MPa. It means that neutral rails temperature is different that assumed one. Variations from assumed neutral temperature are about ±10°C.

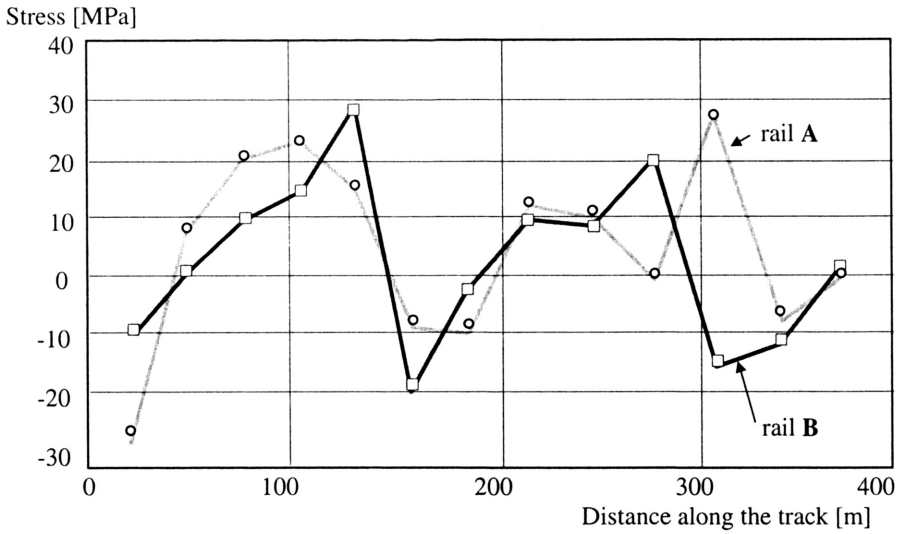

FIGURE 15. Longitudinal stress along the 400 m long segment of CWR at "neutral temperature".

Similar distribution of longitudinal forces in both rails denotes that they were introduced into the CWR during track geometry regulation, when both rails were lifted and displaced together with the ties simultaneously.

The measurements presented in Fig. 15 were performed in July. After 13 months of track service, in October next year, the measurements were repeated in the rail **A**. Results are presented in Fig. 16 where dashed line shows result of measurements performed

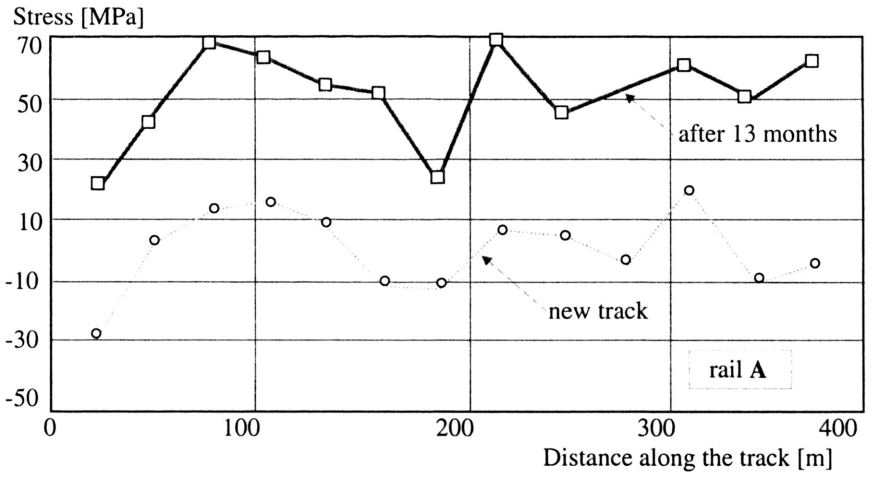

FIGURE 16. Longitudinal stress along the 400 m long segment of CWR measured after 13 months of track service.

in July, on new track. Lower rail temperature in October resulted in more tensile stresses in the rail. The averaged stress difference between July and October measurements is 28 MPa.

The temperature of the rail in October was about 15°C lower. Similar stress distribution along the rail can be observed with a minimum stress at the beginning of the section, maximum for locations 80-120 m and the second minimum at location 190 m.

4.3. Residual stress evaluation in the railroad rails after straightening

Railroad rail is an example of a product in which high residual stresses exist. They are the result of not uniform plastic deformation of the rail material in course of straightening in the roller straightener, which is the last operation during rail manufacturing. The most important, and dangerous, are tensile longitudinal component of residual stress in the rail head and base as well as compressive component in the rail web. High tensile stresses can lead to crack propagation in the base or rail head and significant gradient of tensile stress can be a source of web cracking (cracking of the rail propagating along the web).

Depending on the straightening procedure residual stresses in the rails can reach elastic limit of the rail steel, it is about 500 MPa.

The measurements were performed with subsurface longitudinal and shear waves. The TOF of longitudinal wave depends on rail material elastic properties and on stress. Low stress sensitive shear wave reports about local variations of elastic properties and is used as a reference wave [12]. Before the measurements the device was calibrated. TOFs for longitudinal and shear waves for stress free state were measured on a fragment of the rail after heat relieving annealing.

Figure 17 presents longitudinal component of residual stresses in two rails before straightening. These stresses are result of material deformation during shape rolling and air cooling of the rail. Measurements were performed in four locations on the rail profile:

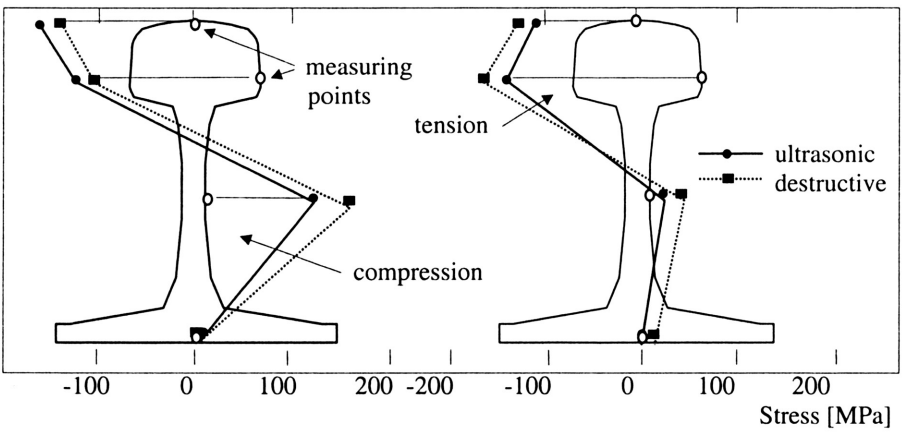

FIGURE 17. Longitudinal residual stresses in two rails before straightening. (Measured in Thionville, France [13]).

head running surface, head side, web and base underside. Solid line on the diagram represents results of ultrasonic measurements, dashed one – results of destructive tests (strain gauges around the circumference and slice cutting).

Compressive stress in the rail head, tensile stress in the web and close to zero stress in the base can be noticed.

Next drawing, Fig. 18, presents results of measurements performed on rails straightened in two different roller straightening machines. Ultrasonic readings were compared with results obtained with destructive measurements. In straightened rail typical stress distribution is observed – tensile stresses in the head running surface and in the base.

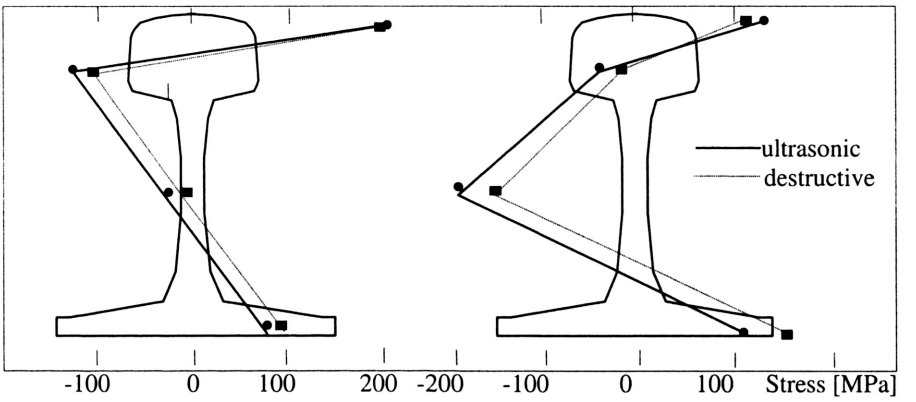

FIGURE 18. Residual stresses in rails straightened in two different straightening machines. (Measured in Thionville, France [13]).

Results presented above were obtained with the device calibrated on the stress free rail sample. Data collected on various straightened rails (as in Fig. 18 for example) showed that on the profile of the straightened rails there are two locations where longitudinal component of residual stress on the rail surface is close to zero. These locations, lower part of the head side and upper part of the rail base, can be used as a zero stress reference area for fast calibration of the device without the need for time consuming and expensive preparation of stress free rail sample. Such a way of calibration was proposed by German and British researchers [14] evaluating stresses with ultrasonic technique. Figure 19 shows results of ultrasonic stress evaluation performed without any calibration on stress free block. Readings were taken on web upper part, web center and on base upper side.

Calculated was averaged stress value U as:

$$U = CW - \frac{UW + UF}{2},$$

where:
CW – reading in web center,
F – on base upperside,
UW – reading on web upperside.

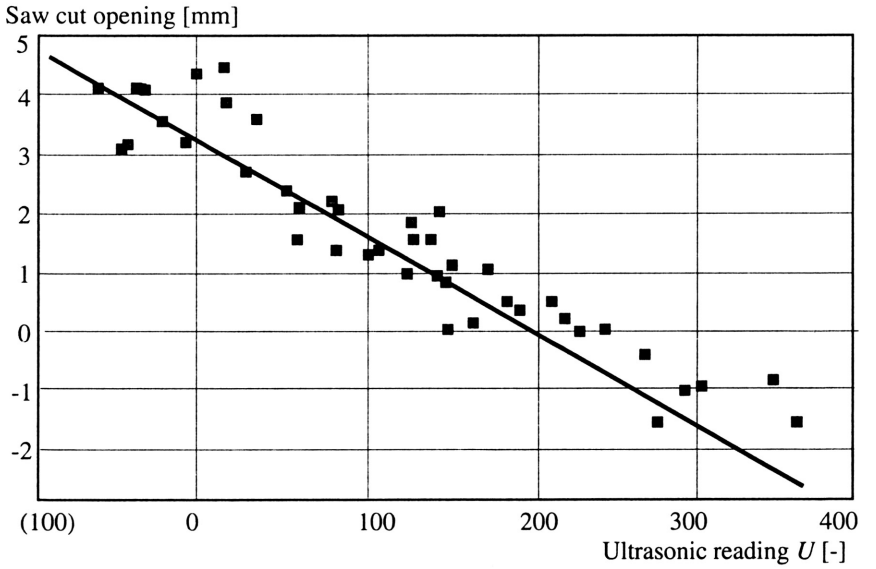

FIGURE 19. Comparison of data obtained with subsurface longitudinal waves measured in three location on the rail profile with destructive, saw cut opening test.

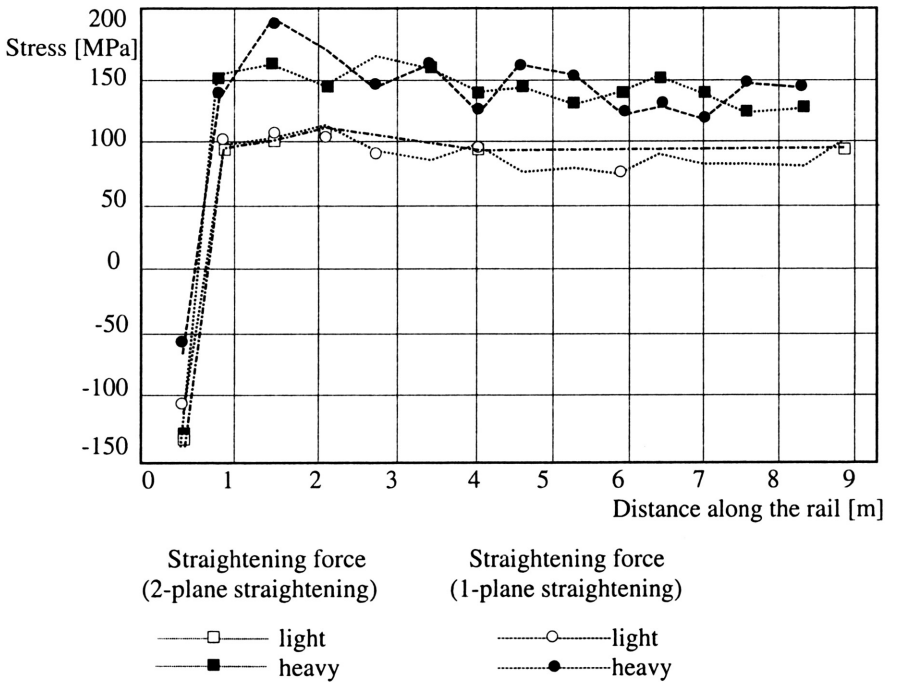

FIGURE 20. Stresses measured along the head running surface on rails straightening under different conditions. (Measured by D. Utrata, Association of American Railroads [15]).

Figure 19 shows comparison of residual "averaged" stress U measured with subsurface waves and saw cut opening (SCO). SCO is the opening of the cut performed along the rail web and is proportional to the values of residual stress difference, or crack driving force, in the rail. This destructive technique was often used as a technological measure of residual longitudinal stress in the rail. Results presented in Fig. 19 were collected by British Steel researchers.

Ultrasonic measurements are fast and, in contrast to resistance strain gauges, can be performed in numerous locations. These features enable evaluation of stress distribution along the rail for example. Figure 20 presents result of such measurements performed along the 9 m long section of the straightened rail. Measurements were taken on rails subjected to various straightening procedures (one and two plane straightening, various roller forces). The readings were taken on the rail head running surface. It can be seen that stress values depend on straightening force.

For rails straightened with higher forces stresses are about 60 MPa higher. Stress variations along the rail are small except leading end of the rail. The ends of the rail,

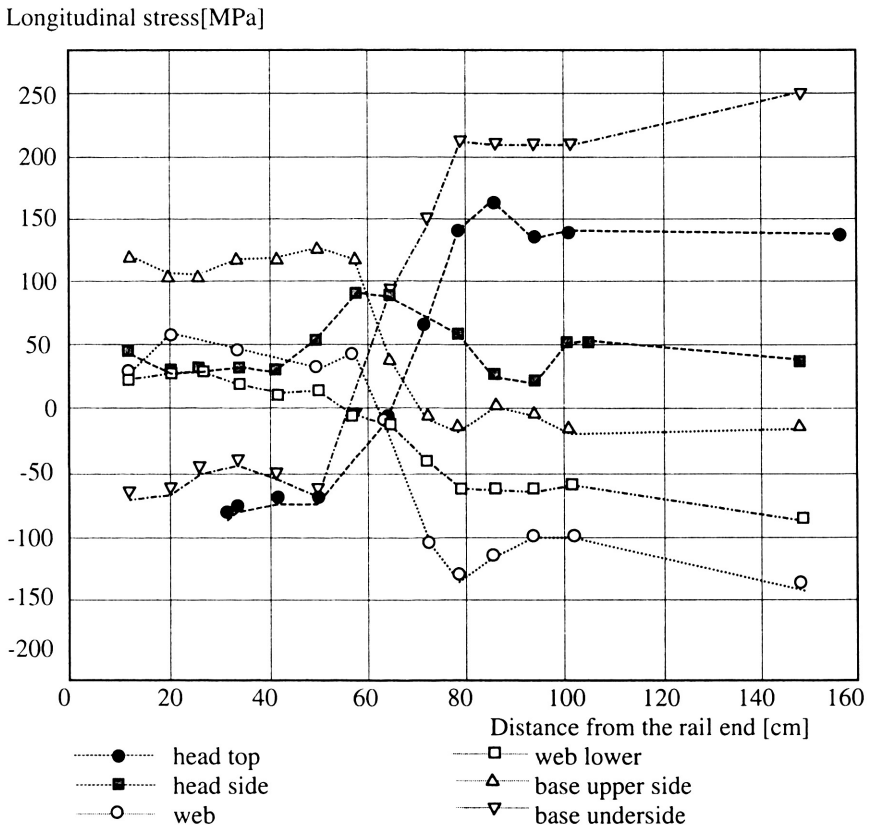

FIGURE 21. The distribution of longitudinal residual stress along the leading end of the rail. (Measured in Association of American Railroads, Chicago [15]).

shorter than the distance between rolls of straightening machine, are not straightened and exhibit stress state as before straightening (compressive stress in the head). More detail stress distribution in this part of the rail is presented in Fig. 21. In this experiment stress was measured not only along the rail running surface but in seven locations around the rail profile.

Compressive longitudinal stresses in the rail head and tensile stress in the rail base, at the beginning of the rail, can be seen. This stress profile is drastically changed by the rolls of the straightening machine as it can be seen for the distances longer than 80 cm from the rail end.

Data presented in Fig. 21 were collected during about 2 hour measurement with ultrasonic device equipped with subsurface waves probehead. It is worth to mention that to collect the same amount of data with strain gauges for example it would be necessary to position about 100 gauges on the rail and to make 28 cuts across the rail.

5. Conclusions

Ultrasonic stress evaluation proved to provide with reliable information concerning stress absolute values of stress and stress changes. However its today applications are limited to heavy steel objects like rails, wheels or shafts subjected to simple stress states. Ultrasonic method is accepted as reliable tool for hoop stress evaluation in monoblock wheels. In many workshops in Europe ultrasonic portable devices are in use today to eliminate dangerous, overheated and stressed wheels from service.

Results of longitudinal force monitoring in CWR, presented in the paper, are not compared with other nondestructive method because ultrasonic technique seems to be today the only one which can be used on various rails, in field conditions, without special rail preparation before measurement. For example, to compare ultrasonic data obtained during track construction with resistance strain gauges technique, more than 200 strain gauges should be glued to the rail. All of gauges should be covered with strong boxes to survive construction works and should be in service for more than one year. Experiment showed also that the exact zero force temperature of CWR is not always known and can vary along the rail. Force gradient in the rail at neutral temperature can be high – up to 300 kN per 100 m.

Experiments with the surface waves for dynamic loads monitoring in bridges structures are carried out [16]. One more successful application of ultrasonic tensometry is evaluation of longitudinal component of residual stress distributions in shafts. Measurements in main propeller shafts [17], as well as all presented in the paper measurements, were performed with the devices designed and built in the IFTR.

References

1. D.A. HUGHES and G.S. KELLY, *Second-Order Elastic Deformation of Solids*, Physical Review, Vol.92, p.1145, 1953.

2. R.N. THURSTON and K. BRUGGER, *Third Order Elastic Constants and Velocity of Small Amplitude Elastic Waves in Homogeneously Stressed Media*, Phys. Rev. A, Vol.133, A1604, 1964.

3. J. DEPUTAT, *Elastoacoustic Phenomena and Its Application for Residual Stress Evaluation* [in Polish], IFTR Report, No.28/1987.

4. A. BROKOWSKI and J. SZELĄŻEK, *Set of Ultrasonic Probeheads for the Measurement of Time of Flight of Ultrasonic Pulses*, Patent USA, No 5,549,001, August 27, 1996.

5. J. SZELĄŻEK, *Ultrasonic Probe for Acoustic Birefringence Measurement* [in Polish], Polish Patent No PL 167941, October 22, 1995.

6. *Effect of Frequent Braking on Residual Stress Field in the Wheel Rim*, Office of Research and Experiments UIC, B-169 Report 2, Utrecht 1989.

7. R.E. SCHRAMM, J. SZELĄŻEK and A.V. CLARK, *Residual Stress in Induction-Heated Railroad Wheels: Ultrasonic and Saw Cut Measurements*, NISTIR 5038, Report No.28, National Institute of Standards and Technology, Boulder, Colorado, May 1995.

8. S.A. PERFECT, *Stress Changes in Railroad Wheels Due to Axially Symmetric Thermal Loads*, Thesis, University of Illinois at Urbana-Champaign, 1980.

9. D. UTRATA, *Longitudinal Rail Stress Measurements Using the Debro-30 Device Technology Digest*, Association of American Railroads, Research and Test Department, Chicago, August 1993.

10. K. TOWPIK and M. ADAMSKI, *Measurements of Continuously Welded Rail Neutral Temperature* [in Polish], Proc. IX Conf. "Railroads", Politechnika Krakowska, pp.333-344, Koscielisko, November 5-7, 1997.

11. J. SZELĄŻEK, *Ultrasonic Measurement of Thermal Stresses in Continuously Welded Rails*, NDT&E International, Vol.25, No.2, pp.77-85, 1992.

12. A. BROKOWSKI and J. DEPUTAT, *Ultrasonic Measurement of Residual Stress in Rails*, Proc. 11 World Conference on Nondestructive Testing, Vol.1, Taylor Publ. Co. Dallas, Las Vegas 1985.

13. *Measures des Contraintes Residuelles dans les Rails par Ultra Sons*, Raport UNIMETAL, March 1989.

14. *Investigations concernant la mesure et l'ammelioration du niveau des contraintes residuelles*, Raport ORE D156,RP, Utracht, September 1987.

15. *Experience with two ultrasonic-based measurement techniques for residual stress determination in railroad rails*, American Railway Engineering Association, Bulletin 733, by Dave Utrata, Chicago 1989.

16. A.V. CLARK, P. FUCH and S.R. SCHAPS, *Fatigue Load Monitoring in Steel Bridges with Rayleigh Waves*, Journal of Nondestructive Evaluation, Vol.14, No.3, pp.83-98, 1995.

17. J. DEPUTAT, M. ADAMSKI, J. GOLJASZ and J. KALISIEWICZ, *Ultrasonic Technique for Investigation of Residual Stresses in Cylindrical Forgings*, Engineering Trans., IFTR, Vol.41, pp.61-67.